Significantly Fast and Robust Fuzzy C-Means Clustering Algorithm Based on Morphological Reconstruction and Membership Filtering

Tao Lei [ORCID], Xiaohong Jia, Yanning Zhang, *Senior Member, IEEE*, Lifeng He, *Senior Member, IEEE*, Hongying Meng [ORCID], *Senior Member, IEEE*, and Asoke K. Nandi [ORCID], *Fellow, IEEE*

Abstract—As fuzzy c-means clustering (FCM) algorithm is sensitive to noise, local spatial information is often introduced to an objective function to improve the robustness of the FCM algorithm for image segmentation. However, the introduction of local spatial information often leads to a high computational complexity, arising out of an iterative calculation of the distance between pixels within local spatial neighbors and clustering centers. To address this issue, an improved FCM algorithm based on morphological reconstruction and membership filtering (FRFCM) that is significantly faster and more robust than FCM is proposed in this paper. First, the local spatial information of images is incorporated into FRFCM by introducing morphological reconstruction operation to guarantee noise-immunity and image detail-preservation. Second, the modification of membership partition, based on the distance between pixels within local spatial neighbors and clustering centers, is replaced by local membership filtering that depends only on the spatial neighbors of membership partition. Compared with state-of-the-art algorithms, the proposed FRFCM algorithm is simpler and significantly faster, since it is unnecessary to compute the distance between pixels within local spatial neighbors and clustering centers. In addition, it is efficient for noisy image segmentation because membership filtering are able to improve membership partition matrix efficiently. Experiments performed on synthetic and real-world images demonstrate that the proposed algorithm not only achieves better results, but also requires less time than the state-of-the-art algorithms for image segmentation.

Index Terms—Fuzzy c-means clustering (FCM), image segmentation, local spatial information, morphological reconstruction (MR).

I. INTRODUCTION

IMAGE segmentation aims to partition an image into several regions that are nonoverlapped and consistent according to the requirements of different applications, and it is always one of the most challenging tasks in image understanding and computer vision due to the variety and complexity of images [1], [2]. Even though numerous approaches [3]–[6] of image segmentation have been proposed, none of them are sufficiently robust and efficient for a large number of different images. The technologies of image segmentation involve clustering [7], [8], region growth [9], watershed transform [10], active contour model [11], MeanShift [12], Graph Cut [13], spectral clustering [14], Markov random field [15], neural network [16], etc. Among these technologies, clustering is one of the most popular methods used for image segmentation because of its effectiveness and rapidity. The aim of clustering is to partition a set into some clusters so that members of the same cluster are similar, and members of different cluster are dissimilar. Generally, clustering methods can be categorized into hierarchical, graph theoretic, decomposing a density function, and minimizing an objective function. In this paper, we will focus on image segmentation based on clustering methods by minimizing an objective function.

As conventional clustering is crisp or hard, it leads to poor results for image segmentation. Based on fuzzy set theory, fuzzy c-means clustering (FCM) had been proposed by Bezdek [17]. FCM is superior to hard clustering as it has more tolerance to ambiguity and retains more original image information. Even though FCM is efficient for images with simple texture and background, it fails to segment images with complex texture and background or images corrupted by noise because it only considers gray-level information without considering the spatial information. To address the problem, one of the most popular ideas is to incorporate the local spatial information in an objective function to improve the segmentation effect. Motivated by this idea, Ahmed *et al*. [18] proposed FCM algorithm with

spatial constraints (FCM_S), where the objective function of the classical FCM is modified in order to take into account of the intensity inhomogeneity and to allow the labeling of a pixel to be influenced by the labels in its immediate neighborhood. However, FCM_S is time-consuming because the spatial neighbors term is computed in each iteration. To reduce the execution time of FCM_S, Chen and Zhang [19] employed average filtering and median filtering to obtain the spatial neighborhood information in advance. Their two proposed variants, FCM_S1 and FCM_S2, have a lower computational cost than FCM_S, since both mean-filtered images and median-filtered images can be computed before the start of the iterative stage. However, both FCM_S1 and FCM_S2 are not robust for Gaussian noise, as well as for known noise intensity. Moreover, it is difficult to ascertain the type of noise and intensity before using FCM_S1 or FCM_S2.

Enhanced FCM (EnFCM) [20] is an excellent algorithm from the viewpoint of its low computational time; it performs clustering based on gray level histograms instead of pixels of a summed image. The computational time is low because the number of gray levels in an image is generally much smaller than the number of its pixels. However, the segmentation result produced by EnFCM is only comparable to that produced by FCM_S. To improve the segmentation results obtained by En-FCM, Cai *et al.* [21] proposed the fast generalized FCM algorithm (FGFCM) that introduced a new factor as a local similarity measure aiming to guarantee both noise-immunity and detail-preservation for image segmentation, and meanwhile removes the empirically-adjusted parameter α that is required in En-FCM, and finally performs clustering on gray level histograms. Although FGFCM is able to improve the robustness and computational efficiency of FCM to some extent, they require more parameters than EnFCM.

To develop new FCM algorithms, which are free from any parameter selection, Krinidis and Chatzis [22] proposed a robust fuzzy local information c-means clustering algorithm (FLICM) by replacing the parameter α employed by EnFCM with a novel fuzzy factor that is incorporated into objective function to guarantee noise-immunity and image detail-preservation. Although the FLICM overcomes the problem of parameter selection and promotes the image segmentation performance, the fixed spatial distance is not robust for different local information of images. Gong *et al.* [23] utilized a variable local coefficient instead of the fixed spatial distance, and proposed a variant of the FLICM algorithm (RFLICM) that is able to exploit more local context information in images. Furthermore, by introducing a kernel metric to FLICM, and employing a tradeoff weighted fuzzy factor to control adaptively the local spatial relationship, Gong *et al.* [24] proposed a novel FCM with local information and kernel metric (KWFLICM) to enhance the robustness of FLICM to noise and outliers. Similar to FLICM, KWFLICM is also free of any parameter selection. However, KWFLICM has a higher computational complexity than FLICM. In fact, the parameter selection depends on image patches and local statistics.

Image patches have been successfully used in nonlocal denoising [25], [26] and texture feature extraction [27], and a higher classification accuracy can be obtained by using the

similarity measurement based on patch. Therefore, patch-based denoising methods, where the nonlocal spatial information is introduced in an objective function by utilizing a variant parameter, which is adaptive according to noise level for each pixel of images [24], are extended to FCM to overcome the problem of parameter selection to improve the robustness to noise. However, it is well known that patch-based nonlocal filtering and parameter estimation have a very high computational complexity. To reduce the running time of FLICM and KWFLICM, Zhao *et al.* [28] proposed neighborhood weighted FCM algorithm (NWFCM) that replaces the Euclidean distance in the objective function of FCM with a neighborhood weighted-distance obtained by patch distance. Even though the NWFCM is faster than FLICM and KWFLICM, it is still time-consuming because of the calculation of patch distance and parameter selection. To overcome the shortcoming, Guo *et al.* [29] proposed an adaptive FCM algorithm based on noise detection (NDFCM), where the tradeoff parameter is tuned automatically by measuring local variance of grey levels. Despite the fact that NDFCM employs more parameters, it is fast since image filtering is executed before the start of iterations.

Following the work mentioned above, in this study, we propose a significantly fast and robust algorithm for image segmentation. The proposed algorithm can achieve good segmentation results for a variety of images with a low computational cost, yet achieve a high segmentation precision.

Our main contributions can be summarized as follows.

1) The proposed FRFCM employs morphological reconstruction (MR) [30], [31] to smooth images in order to improve the noise-immunity and image detail-preservation simultaneously, which removed the difficulty of having to choose different filters suitable for different types of noise in existing improved FCM algorithms. Therefore, the proposed FRFCM is more robust than these algorithms for images corrupted by different types of noise.

2) The proposed FRFCM modifies membership partition by using a faster membership filtering instead of the slower distance computation between pixels within local spatial neighbors and their clustering centers, which leads to a low computational complexity. Therefore, the proposed FRFCM is faster than other improved FCM algorithms.

The rest of this paper is organized as follows. In Section II, we provide the motivation for our work. In Section III, we propose our algorithm and model. The experimental results on synthetic images, real medical images, aurora images, and color images are described in Section IV, Finally, we present our conclusion in Section V.

II. MOTIVATION

To improve the drawback that FCM algorithm is sensitive to noise, most algorithms try to overcome the drawback by incorporating local spatial information to FCM algorithm, such as FLICM, KWFLICM, NWFCM, etc. However, a high computational complexity is a problem for them. In fact, the introduction of local spatial information is similar to image filtering in advance (see Appendix A). Thus, local spatial information of an

image can be calculated before applying the FCM algorithm, which will efficiently reduce computational complexity, such as FCM_S1 and FCM_S2. Besides, if the membership is modified through the use of the relationship of the neighborhood pixels, but the objective function is not modified, then the corresponding algorithm will be simple and fast [32]. Motivated by this, in this paper, we improve FCM algorithm in two ways: one is to introduce local spatial information using a new method with a low computational complexity and the other is to modify pixels' membership without depending on the calculation of distance between pixels within local spatial neighbors and clustering centers. The proposed algorithm on image segmentation will be implemented efficiently with a small computational cost.

A. Motivation of Using MR

By introducing local spatial information to an objective function of FCM algorithm, the improved FCM algorithms are insensitive to noise and show better performance for image segmentation. Generally, the modified objective function of these algorithms is given as follows:

$$J_m = \sum_{i=1}^{N} \sum_{k=1}^{c} u_{ki}^m \|x_i - v_k\|^2 + \sum_{i=1}^{N} \sum_{k=1}^{c} G_{ki} \tag{1}$$

where $f = \{x_1, x_2, \cdots, x_N\}$ represents a grayscale image, x_i is the gray value of the ith pixel, v_k represents the prototype value of the kth cluster, u_{ki} denotes the fuzzy membership value of the ith pixel with respect to cluster k. $\boldsymbol{U} = [u_{ki}]^{c \times N}$ represents membership partition matrix. N is the total number of pixels in the image f, and c is the number of clusters. The parameter m is a weighting exponent on each fuzzy membership that determines the amount of fuzziness of the resulting classification. The fuzzy factor G_{ki} is used to control the influence of neighborhood pixels on the central pixel. Different G_{ki} usually leads to variant clustering algorithms, such as FCM_S, FCM_S1, FCM_S2, FLICM, KWFLICM, NWFCM, etc. From these algorithms, we found that the form of G_{ki} directly decides the computational complexity of different clustering algorithms. For example, in FCM_S, the G_{ki} is defined as

$$G_{ki} = \frac{\alpha}{N_R} u_{ki}^m \sum_{r \in N_i} \|x_r - v_k\|^2 \tag{2}$$

where α is a parameter that is used to control the effect of the neighbors term, N_R is the cardinality of u_{ki}, x_r denotes the neighbor of x_i, and N_i is the set of neighbors within a window around x_i.

For FLICM, the G_{ki} is defined as

$$G_{ki} = \sum_{\substack{r \in N_i \\ i \neq r}} \frac{1}{d_{ir} + 1} \left(1 - u_{kr}\right)^m \|x_r - v_k\|^2 \tag{3}$$

where d_{ir} represents the spatial Euclidean distance between pixels x_i and x_r. It is obvious that the G_{ki} is more complex than that in FCM_S, and thus FLICM has a higher computational complexity than FCM_S. In FCM_S1 and FCM_S2, the G_{ki} is defined as

$$G_{ki} = \alpha u_{ki}^m \|\hat{x}_i - v_k\|^2 \tag{4}$$

where $\hat{x}_i$ is a mean value or median value of neighboring pixels lying within a window around x_i. The G_{ki} in FCM_S1 and FCM_S2 has a more simplified form than FCM_S, and the clustering time can be reduced because $\sum_{r \in N_i} \|x_r - u_k\|^2 / N_R$ is replaced by $\alpha \|\hat{x}_i - u_k\|^2$.

Although FCM_S1 and FCM_S2 simplified the neighbors term in the objective function of FCM_S, and presented excellent performance for image segmentation, it is difficult to ascertain noise type that is required to choose a suitable filter (mean or median filter). FCM_S2 is able to obtain good segmentation results for images corrupted by Salt & Pepper noise, but it is incapable of doing so for images corrupted by Gaussian noise. FCM_S1 produces worse results compared with FCM_S2. In practical applications, we expect to obtain a robust $\hat{x}$ in which different types of noise are efficiently removed while image details are preserved. Motivated by this, we introduce MR to FCM because MR is not only able to obtain a good result, but also it requires a short running time [33]. Therefore, in this paper, we introduce MR to FCM to address the drawback produced by conventional filters. MR uses a marker image to reconstruct original image to obtain a better image, which is favorable to image segmentation based on clustering. Similar to FCM_S1 and FCM_S2, the reconstructed image will be computed in advance, and thus the computational complexity of the proposed algorithm is low. We will present the computation of reconstructed image in details in Section III.

B. Motivation of Using Membership Filtering

In FCM algorithm, according to the definition of the object function and the constraint that $\sum_{k=1}^{c} u_{ki} = 1$ for each pixel x_i, and using the Lagrange multiplier method, the calculations of membership partition matrix and the clustering centers are given as follows:

$$u_{ki} = \frac{\|x_i - v_k\|^{-2/(m-1)}}{\sum_{j=1}^{c} \|x_i - v_j\|^{-2/(m-1)}} \tag{5}$$

$$v_k = \frac{\sum_{i=1}^{N} u_{ki}^m x_i}{\sum_{i=1}^{N} u_{ki}^m}. \tag{6}$$

According to (5), it is easy and fast to compute u_{ki} by using vector operation for FCM algorithm. However, it is complex and slow to compute u_{ki} shown in (7) for improved FCM algorithm, such as FLICM and KWFLICM because vector operation cannot be used in the computation of G_{ki} in (3).

$$u_{ki} = \frac{\left(\|x_i - v_k\|^2 + G_{ki}\right)^{-1/(m-1)}}{\sum_{j=1}^{c} \left(\|x_i - v_j\|^2 + G_{ji}\right)^{-1/(m-1)}}. \tag{7}$$

Therefore, multiple loop program is employed by FLICM and KWFLICM, which causes a high computational complexity. On the one hand, the introduction of G_{ki} in (7) is able to improve the robustness of FCM to noisy image segmentation, but on the other hand, the introduction of G_{ki} causes a high computational cost. Clearly, there is a contradiction between improving the robustness and reducing the computational complexity simultaneously for FCM [34]. We found that if G_{ki} can be computed in advance, the contradiction will disappear because the u_{ki} in

(7) can be computed by using vector operation without multiple loops.

In this paper, we introduce membership filtering to FCM to address the contradiction mentioned above. First, because a reconstructed image is computed in advance, we perform clustering on the gray level histogram of an image reconstructed by MR. After obtaining fuzzy membership partition matrix, we use membership filtering to modify membership partition matrix to avoid the computation of distance between pixels within local spatial neighbors and clustering centers. We present our proposed method in details in Section III.

III. METHODOLOGY

In this study, we employ MR to replace mean or median filters due to its robustness to noise. MR is able to efficiently suppress different noise without considering noise type. Moreover, MR algorithm is fast as parallel algorithms exist for the implementation of MR. Motivated by the idea of EnFCM, we perform clustering on the gray level histogram of an image reconstructed by MR to obtain a fuzzy membership matrix via iteration operation. Finally, a filter is employed to modify the membership partition matrix. Using this method, we can obtain a good segmentation result requiring less time.

A. General Overview of the Proposed Methodology

Similar to EnFCM, the clustering of the proposed FRFCM is performed on the gray level histogram, and thus the objective function can be written as

$$J_m = \sum_{l=1}^{q} \sum_{k=1}^{c} \gamma_l u_{kl}^m \| \xi_l - v_k \|^2 \tag{8}$$

where u_{kl} represents the fuzzy membership of gray value l with respect to cluster k, and

$$\sum_{l=1}^{q} \gamma_l = N \tag{9}$$

where ξ is an image reconstructed by MR, and ξ_l is a gray level, $1 \leqslant l \leqslant q$, q denotes the number of the gray levels contained in ξ, it is generally much smaller than N. ξ is defined as follows:

$$\xi = R^C(f) \tag{10}$$

where R^C denotes morphological closing reconstruction and f represents an original image.

Utilizing the Lagrange multiplier technique, the aforementioned optimization problem can be converted to an unconstrained optimization problem that minimizes the following objective function:

$$\tilde{J}_m = \sum_{l=1}^{q} \sum_{k=1}^{c} \gamma_l u_{kl}^m \| \xi_l - v_k \|^2 - \lambda \left(\sum_{k=1}^{c} u_{kl} - 1 \right) \tag{11}$$

where λ is a Lagrange multiplier. Therefore, the problem of the minimization of objective function is converted to finding the saddle point of the above Lagrange function and taking the derivatives of the Lagrangian $\tilde{J}_m$ with respect to the parameters, i.e., u_{kl} and v_k.

By minimizing the objective function (8), we obtained the corresponding solution as follows:

$$u_{kl} = \frac{\| \xi_l - v_k \|^{-2/(m-1)}}{\sum_{j=1}^{c} \| \xi_l - v_j \|^{-2/(m-1)}} \tag{12}$$

$$v_k = \frac{\sum_{i=1}^{q} \gamma_l u_{kl}^m \xi_l}{\sum_{i=1}^{q} \gamma_l u_{kl}^m}. \tag{13}$$

According to (12), a membership partition matrix $U = [u_{kl}]^{c \times q}$ is obtained. To obtain a stable U, (12) and (13) are repeatedly implemented until $\max\{U^{(t)} - U^{(t+1)}\} < \eta$, where η is a minimal error threshold. Because $u_{kl}^{(t)}$ is a fuzzy membership of gray value l with respect to cluster k, a new membership partition matrix $U' = [u_{kl}]^{c \times N}$ that corresponds to the original image f, is obtained, i.e.,

$$u_{ki} = u_{kl}^{(t)}, \text{ if } x_i = \xi_l. \tag{14}$$

To obtain a better membership partition matrix and to speed up the convergence of our algorithm, we modify u_{ki} by using membership filtering. Considering the tradeoff between performance of membership filtering and the speed of algorithms, we employ a median filter in this paper as follows:

$$U'' = \text{med}\{U'\} \tag{15}$$

where med represents median filtering.

Based on the analysis mentioned above, the proposed algorithm FRFCM can be summarized as follows.

Step 1: Set the cluster prototype value c, fuzzification parameter m, the size of filtering window w, and the minimal error threshold η.

Step 2: Compute the new image ξ using (10), and then compute the histogram of ξ.

Step 3: Initialize randomly the membership partition matrix $U^{(0)}$.

Step 4: Set the loop counter $t = 0$.

Step 5: Update the clustering centers using (13).

Step 6: Update the membership partition matrix $U^{(t+1)}$ using (12).

Step 7: If $\max\{U^{(t)} - U^{(t+1)}\} < \eta$ then stop, otherwise, set $t = t + 1$ and go to Step 5.

Step 8: Implement median filtering on membership partition matrix U' using (15).

B. Morphological Reconstruction

For FCM algorithm, the rate of convergence is always decided by the distribution characteristics of data. If the distribution characteristic of data is favorable to clustering, the corresponding number of iterations is small, otherwise, the number of iterations is large. FCM is sensitive to noise because the distribution characteristics of data is always affected by noise corruption, which causes two problems. One is that the result obtained by FCM algorithm is poor for noisy image segmentation; the other is that the number of iterations of FCM is larger for an image corrupted by noise than the image uncorrupted by noise. It is well known that the distribution characteristic of data can be described by histogram. If the histogram is uniform, it is difficult to achieve a good and fast image segmentation. On the
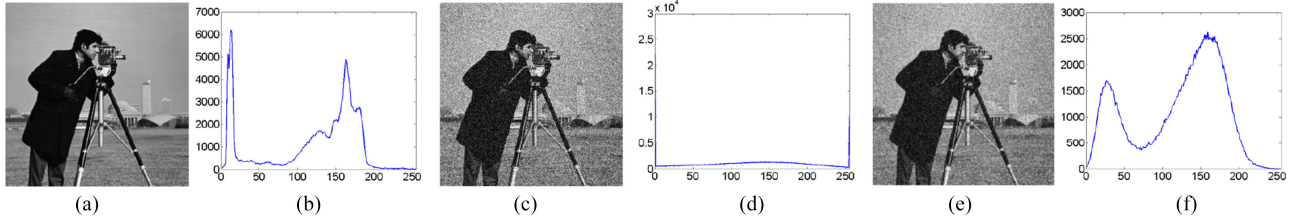
Fig. 1. Comparison of distribution characteristics of data for noisy image and filtered image. (a) Original imge "cameraman" (image size: 512×512). (b) Histogram of the original image. (c) Image corrupted by Gaussian noise (the mean value is zero, and the variance is 5%) (d) Histogram of (c). (e) image filtered by a mean filter (3×3). (f) Histogram of (e).

TABLE I
COMPARISON OF NUMBER OF ITERATIONS FOR THREE DIFFERENT IMAGES (THE NUMBERS REPRESENT THE AVERAGES OF REPEATING 100 TIMES)

	Original image [Fig. 1(a)]	Noisy image [Fig. 2(a)]	Filtered image [Fig. 2(c)]
Numbers of iterations with standard deviations	21.06 ± 1.91	38.46 ± 7.51	24.56 ± 1.48

contrary, it is easy if the histogram has several apparent peaks. Fig. 1 shows an example.

Fig. 1 shows that the histogram of original image has two obvious peaks while the histogram of image corrupted by Gaussian noise has no obvious peaks except extremum (0 and 255). There are two obvious peaks in Fig. 1(f), similar to the original Fig. 1(b), demonstrating a mean filter is efficient for the removal of Gaussian noise. We implemented FCM algorithm on three images: original image, the image corrupted by Gaussian noise (the mean vlaue is zero, and the variance is 5%), and the image filtered by a mean filter (the size of the filtering window is 3×3). Table I shows the comparison of number of iterations of FCM for the three images ($c = 2$).

Table I shows that the number of iterations of FCM is the smallest for the original image and it is the largest for the noisy image. Mean filter is efficient for the optimization of data distribution because the number of iterations is reduced.

In this paper, we introduce MR to FCM algorithm to optimize distribution characteristic of data before applying clustering. MR is able to preserve object contour and remove noise without knowing the noise type in advance [35], which is useful for optimizing distribution characteristic of data.

There are two basic MR operations, morphological dilation and erosion reconstructions [36]. Morphological dilation reconstruction is denoted by $R_f^\delta(g)$ that is defined as

$$R_f^\delta(g) = \delta_f^{(i)}(g) \tag{16}$$

where f is the original image, g is a marker image and $g \leqslant f$, δ represents dilation operation, and $\delta_f^{(1)}(g) = \delta(g) \wedge f, \delta_g^{(i)}(f) = \delta(\delta^{(i-1)}(g)) \wedge f$, and $\wedge$ stands for the pointwise minimum.

By duality, morphological erosion reconstruction is denoted by $R_f^\varepsilon(g)$ that is defined as

$$R_f^\varepsilon(g) = \varepsilon_f^{(i)}(g) \tag{17}$$

where $g \geqslant f$, ξ represents erosion operation, and $\varepsilon_f^{(1)}(g) = \varepsilon(g) \vee f$, $\varepsilon_g^{(i)}(f) = \varepsilon(\varepsilon^{(i-1)}(g)) \vee f$, and $\vee$ stands for the pointwise maximum.

The reconstruction result of an image depends on the selection of marker images and mask images [37]. Generally, if the original image is used as a mask image, then the transformation of the original image is considered as the marker image. In practical applications, $g = \varepsilon(f)$ meets the condition $g \leqslant f$ for dilation reconstructions and $g = \delta(f)$ meets the condition $g \geqslant f$ for erosion reconstructions. Thus, $g = \varepsilon(f)$ and $g = \delta(f)$ are always used to obtain a marker image due to simplicity and effectiveness.

Based on the composition of erosion and dilation reconstructions, some reconstruction operators with stronger filtering capability can be obtained, such as morphological opening and closing reconstructions. Because morphological closing reconstruction, denoted by R^C, is more suitable for texture detail smoothing, we employ R^C to modify original image. R^C is defined as follows:

$$R^C(f) = R_{R_f^\delta(\varepsilon(f))}^\varepsilon \left(\delta \left(R_f^\delta(\varepsilon(f)) \right) \right). \tag{18}$$

In [20], the modified image $\xi = (\xi_i)_{i=1}^N$ is defined as

$$\xi_i = \frac{1}{1+\alpha} (x_i + \alpha \hat{x}_i). \tag{19}$$

According to (18), $x_i \in f$ and $\hat{x}_i \in R^C(f)$, where $R^C(f)$ denotes a reconstructed image obtained by R^C. To obtain a marker image, a structuring element B including center element is required for ε or δ, i.e., $\varepsilon_B(f) \leq f$ and $\delta_B(f) \geq f$. Then, R^C is rewritten as

$$R^C(f) = R_{R_f^\delta(\varepsilon_B(f))}^\varepsilon \left(\delta_B \left(R_f^\delta(\varepsilon_B(f)) \right) \right). \tag{20}$$

For example, a disk with radius r can be considered as B. If $r = 0$, then $R^C(f) = f$; else f will be smoothed to different degree according to the change of r. Therefore, the effect of α is similar to r. And thus, we can replace ξ with $R^C(f)$, and the parameter α will be removed, which solves the problem of noise estimation because MR is able to remove different noises efficiently.

To show the effect of MR for different type of noise removal in images, Fig. 2 shows comparative results generated by a mean
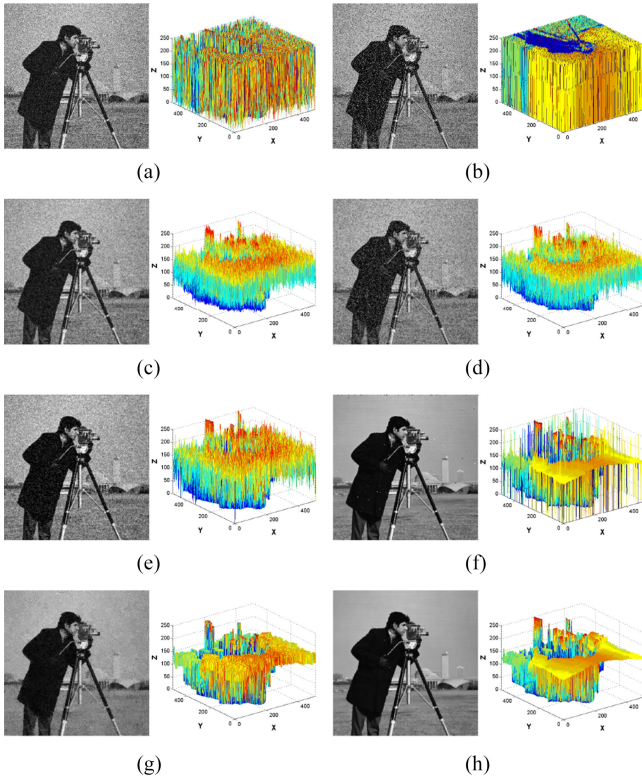
Fig. 2.   Comparison of noise removal using different methods. (a) Image corrupted by Gaussian noise (the mean value is zero, and the variance is 5%). (b) Image corrupted by Salt & Pepper noise (the noise density is 20%). (c) Filtered result using mean filtering for (a). (d) Filtered result using mean filtering for (b). (e) Filtered result using median filtering for (a). (f) Filtered result using median filtering for (b). (g) Filtered result using MR for (a). (h) Filtered result using MR for (b).

Fig. 3.   Comparison of membership partition from FCM and FLICM ($c = 3$, and the iteration step is 10). (a) Original synthetic image included three gray levels (0, 85, 170). (b) Image corrupted by Gaussian noise (the mean value is zero, and the variance is 3%). (c) Membership partition using FCM. (d) Membership partition using FLICM.

filter, a median filter, and R^C. The original image is Fig. 1(a), and the size of the filtering window employed by the mean and the median filters is 3×3. For consistency, the structuring element, in this case, is also a square of size 3×3 ($r = 1$).

Fig. 2(c), (e), and (g) is filtering results of image corrupted by Gaussian noise by using the mean filter, the median filter, and R^C respectively. It is clear that R^C is efficient for Gaussian noise removal. Similarly, Fig. 2(d), (f), and (h) is filtering results of image corrupted by Salt & Pepper noise by using the mean filter, the median filter, and R^C, respectively. It is also clear that R^C is efficient for Salt & Pepper noise removal. Therefore, on the one hand, MR removes the difficulty of choosing filters for images corrupted by noise; on the other hand, MR integrates spatial information into FCM to achieve a better image segmentation. Compared with mean filtering and median filtering, Fig. 2 shows that MR is able to optimize data distribution without considering noise type. Moreover, MR can obtain better results for image filtering than mean and median filters, which is important for subsequent clustering and image segmentation.

C. Membership Filtering

According to the above results in Section III-B, we found that the introduction of local spatial information is useful and efficient for improving FCM algorithm. However, the computation
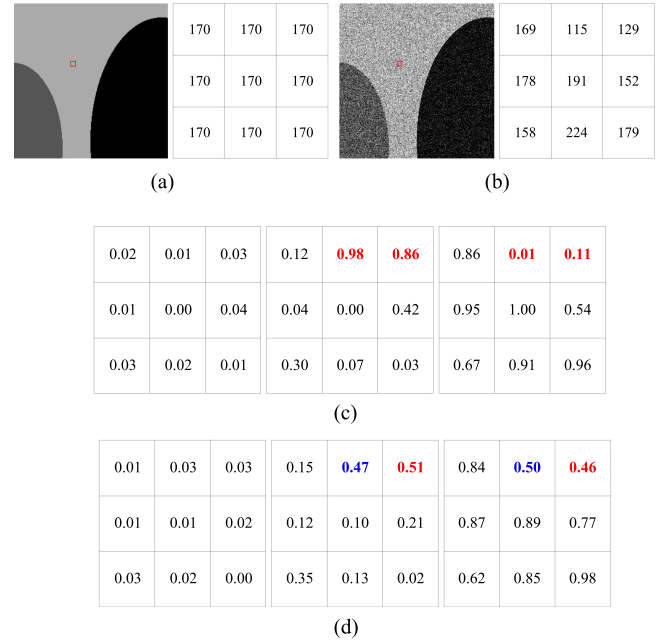
of distance between pixels within local spatial neighbors and clustering centers does introduce a high computational complexity, such as FCM_S. Although some improved algorithms, such as FCM_S1 and FCM_S2, reduce computational complexity by computing spatial neighborhood information in advance, these algorithms need to ascertain the noise type before applying an image filter. To exploit spatial neighborhood information during the iteration process of clustering, FLICM and KWFLICM compute the distance between the neighbors of pixels and clustering centers in each iteration. Although FLICM and KWFLICM produce good segmentation results for noisy images, they have a high computational complexity.

In [22], FLICM will be equal to FCM, if G_{ki} is removed. For this the idea is to replace G_{ki} in a simple way where the computation of distance between pixels within local spatial neighbors and v_k is unnecessary. Motivated by the idea, membership filtering is introduced. We will replace the contribution of G_{ki} with the spatial neighborhood information of membership partition. To further analyze the contribution of G_{ki}, Fig. 3 shows the effect of spatial neighborhood information on membership partition.

FCM and FLICM are used to segment Fig. 3(b). Fig. 3(c) and (d) is membership partition provided by FCM and FLICM, respectively, when the number of iterations is 10. Fig. 3(c) shows that some pixels marked with red color will be misclassified because the original image is corrupted by Gaussian noise. By introducing local spatial information into FLICM, the misclassified pixel will be corrected as shown in Fig. 3(d) (the corrected pixels are marked with blue color). For a pixel (the gray value is 115) in Fig. 3(b), we obtained three fuzzy memberships (0.01,

0.01	0.02	0.02	0.04	**0.04**	**0.07**	0.95	**0.94**	**0.91**
0.01	0.01	0.05	0.04	0.04	0.14	0.95	0.95	0.81
0.02	0.01	0.01	0.04	0.04	0.05	0.94	0.95	0.94

Fig. 4. Membership partition using FCM based on membership filter for Fig. 3(b) (the iteration step is 10).

0.98, 0.01) of the pixel shown in Fig. 3(c) by using FCM, which clearly indicates that the pixel belongs to the second cluster according to FCM. However, in reality, it belongs the third cluster (the gray value is 170) according to the Ground Truth. In Fig. 3(d), we obtained new fuzzy memberships (0.03, 0.47, 0.50) of the pixel by using FLICM, which shows that the pixel belongs the third cluster because 0.5 is the maximal membership. Even though pixels corrupted with Gaussian noise are classified accurately by FLICM, the maximal membership value of pixels is small. And thus, FLICM has a slow speed of convergence.

According to (2) and (7), u_{ki} depends on the distance $\|x_i - v_k\|$ and $\|x_r - v_k\|$. But in fact, $\|x_r - v_k\|$ is a repetitive or redundant computation since it can be obtained according to $\|x_i - v_k\|$. It is the same as KWFLICM. It is clear that we can use a membership filter to correct the misclassified pixels, i.e., it is unnecessary to compute the distance between the neighbors of pixels and clustering centers. According to G_{ki} shown in (3), the modified membership partition is considered as

$$u'_{ki} = u_{ki} + \sum_{\substack{r \in N_i \\ i \neq r}} \frac{1}{d_{ir} + 1} u_{kr} \tag{21}$$

where d_{ir} represents the Euclidean distance between u_{ki} and u_{kr}, and u_{kr} is the neighbors of u_{ki}. The factor, $1/(d_{ir} + 1)$, reflects the spatial structure information of membership partition.

Because FLICM is sensitive to Salt & Pepper noise, it is inefficient to use (21) to remove the noise. In this paper, we use a median filter to modify membership partition as shown in (15), In fact, it can be demonstrated that the introduction of local spatial information is similar to membership filter for improving segmentation results (see in Appendix A). However, membership filtering does not require to compute the distance between the pixels within local spatial neighbors and clustering centers. Therefore, the corresponding computational complexity of improved algorithms based on membership filtering is lower than other algorithms, such as NWFCM, FLICM, KWFLICM, etc. For membership partition obtained by FCM in each iteration shown in Fig. 3, a median filter is used to modify membership partition, and Fig. 4 shows results (the result is normalized, and the filtering window is the same as the structuring element *B*).

Fig. 4 shows membership filtering has a capability of correcting misclassified pixels. Moreover, it provides a better membership partition than FLICM. Therefore, it is a good idea to utilize membership filtering instead of the introduction of fuzzy factor G_{ki}. Also, FCM algorithm based on membership filtering (MFFCM) provides better clustering centers than FCM as shown

in Table II. Therefore, the objective function of FCM algorithm based on membership filtering converges quickly. However, if membership filtering is implemented in each iteration, the corresponding algorithm will be complex and lowly efficient. To improve the computational efficiency of MFFCM further, membership filtering is just implemented once on the final membership partition matrix.

Based on the analysis above, MR is used to optimize data distribution, and then we implement FCM algorithm on the histogram of reconstructed image. Finally, we use a median filter to modify membership partition. The proposed FRFCM is implemented on Fig. 3(b), and Table II shows the comparison of values of clustering centers produced by FCM, FLICM, MFFCM, and FRFCM, where the mean square error (MSE) of clustering centers is used to evaluate the performance of different algorithms.

In Table II, 11.4, 18.9, 18.9, and 5.6 are values of the first clustering center obtained by FCM, FLICM, MFFCM, and FRFCM, respectively. The value, 33.07, is the MSE between the FCM results of (11.4, 106.9, 192.0) and the Ground Truth of (0, 85, 170). It is clear that the value, 5.6, from FRFCM is the closest value to 0 that is the first clustering center from the Ground Truth. Consequently, Table II demonstrates that FRFCM provides the best clustering centers after ten iterations. Based on the analysis mentioned above, we conclude that the proposed FRFCM has following advantages.

1) Similar to FLICM and KWFLICM, it is free from parameters except the size of filtering window.
2) It has a low computational complexity because the redundant computation of distance is unnecessary.
3) It is able to provide good results for image segmentation because of the introduction of MR and membership filtering, and thus spatial information is efficiently exploited.

IV. EXPERIMENTS

To estimate the effectiveness and efficiency of the proposed FRFCM, synthetic noise images, real images including a medical image and an aurora image, and color images are tested in our experiments. Nine state-of-the-art clustering algorithms: FCM [17], FCM_S1 [19], FCM_S2 [19], EnFCM [20], FGFCM [21], FLICM [22], KWFLICM [24], NWFCM [28], and NDFCM [29], are employed in these experiments to compare with the proposed FRFCM. These algorithms have different advantages. FCM, FCM_S1, FCM_S2, EnFCM, FGFCM, and NDFCM have a low computational complexity. FLICM, KWFLICM, and NWFCM have a strong capability of noise removal, while FLICM and KWFLICM do not require parameter values to be set.

In the following experiments, a fixed 3×3 window is used in all the algorithms except FCM for fair comparison. The weighting exponent is set $m = 2$, $\eta = 10^{-5}$. In addition, according to FCM_S1, FCM_S2, and EnFCM, α is used to control the effect of the neighbors term, experientially, $\alpha = 3.8$. In FGFCM and NDFCM, the spatial scale factor and the gray-level scale factor are $\lambda_s = 3$ and $\lambda_g = 5$, respectively. Besides, a new scale factor λ_α equals to 3 for the NDFCM [29]. For NWFCM, λ_g equals to 5. Except m, η, and the number of the cluster prototype,

TABLE II
COMPARISON OF CLUSTERING CENTERS PRODUCED BY DIFFERENT ALGORITHMS [THE DATA REPRESENTS AVERAGE RESULTS OF REPEATING 100 TIMES, THE ITERATION STEP IS 10, AND THREE GRAY LEVELS OF GROUND TRUTH FIG. 3(A) IS (0, 85, 170)]. THE BEST VALUES ARE HIGHLIGHTED.

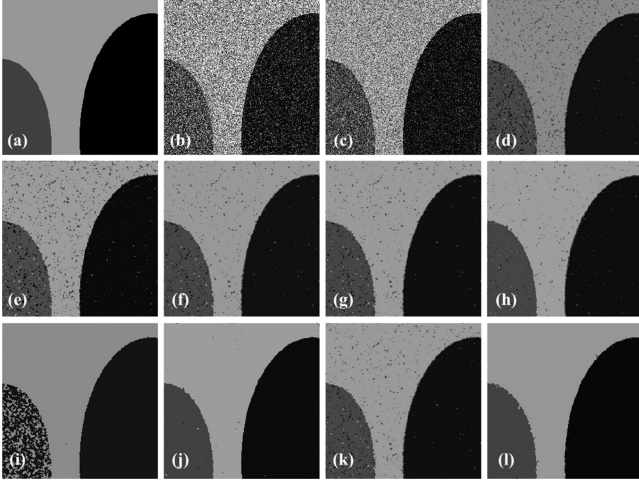| Method	FCM	FLICM	MFFCM	FRFCM
Values of clustering centers	(11.4, 106.9, 192.0)	(18.9, 117.3, 179.1)	(18.9, 91.2, 169.7)	**(5.6, 85.4, 169.1)**
MSE	33.07	38.51	19.89	**5.69**

Fig. 5. Comparison of segmentation results on the first symmetric image. (a) Original image. (b) noisy image (Gaussian noise with zero mean and 5% variance). (c) FCM result. (d) FCM_S1 result. (e) FCM_S2 result. (f) EnFCM result. (g) FGFCM result. (h) FLICM result. (i) NWFCM result. (j) KWFLICM result. (k) NDFCM result. (l) FRFCM result.
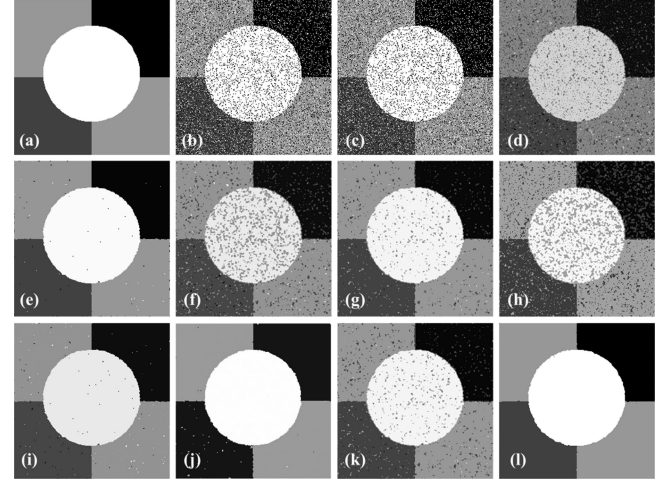

Fig. 6. Comparison of segmentation results on the second symmetric image. (a) Original image. (b) Noisy image (Salt & Pepper, the noise intensity is 20%). (c) FCM result. (d) FCM_S1 result. (e) FCM_S2 result. (f) EnFCM result. (g) FGFCM result. (h) FLICM result. (i) NWFCM result. (j) KWFLICM result. (k) NDFCM result. (l) FRFCM result.

there is no other parameters for FLICM and KWFLICM. For our FRFCM, the mask image is the original image, and a square structuring element of size 3×3 is used to obtain marker image. In addition, median filter is used to fuzzy membership filtering, and the filtering window is also 3×3.

A. Results on Synthetic Images

In this section, two synthetic images with size 256×256 are used in the experiment. The first image includes three classes (three intensity values are 0, 85, and 170, respectively), and the second image includes four classes (four intensity value are 0, 85, 170, and 255, respectively). The two synthetic images are shown in Figs. 5(a) and 6(a), respectively. These images are corrupted by Gaussian, Salt & Pepper, and Uniform noise, respectively, and these corrupted images are utilized for testing the efficiency and robustness of above algorithms. Figs. 5(c-l) and 6(c-l) show segmentation results obtained by different algorithms.

In addition, a performance index, the optimal segmentation accuracy (SA), and a quantitative index score (S) [18], are used to assess the denoising performance of different algorithms, where SA is defined as the sum of the correctly classified pixels divided by the sum of the total number of the pixels

$$SA = \sum_{k=1}^{c} \frac{A_k \bigcap C_k}{\sum_{j=1}^{c} C_j} \tag{22}$$

and S is defined as the degree of equality between pixel sets A_k and the Ground Truth C_k

$$S = \sum_{k=1}^{c} \frac{A_k \bigcap C_k}{A_k \bigcup C_k} \tag{23}$$

where c is the number of the cluster prototype, A_k denotes the set of pixels belonging to the kth class found by the algorithm, while C_k denotes the set of pixels belonging to the class in the Ground Truth. All the algorithms are repeatedly run 100 times on synthetic images corrupted by different noises. Tables III and IV give the average segmentation accuracy and the scores results of the repeated experiments for the ten algorithms.

In Fig. 5, FCM algorithm does not overcome its sensitivity to noise. FCM_S1 and FCM_S2 are able to reduce the effect of noise on segmentation results due to the introduction of local spatial information. EnFCM, FGFCM, and NDFCM improve segmentation results to some extent, the segmented images have better visual effect than FCM, FCM_S1, and FCM_S2. Although NWFCM obtains a better visual effect for the first and the third classes (the clustering centers are 0 and 170), it causes a poor effect on the second class (the clustering center is 85). FLICM and KWFLICM are superior to FGFCM depending on Fig. 5(h) and (j). Fig. 5(l) shows that the proposed FRFCM obtains better segmentation result than other algorithms.

Fig. 6 shows that FCM_S1 obtains a poor segmentation result which is close to FCM because mean filters employed by

TABLE III
SEGMENTATION ACCURACY (SA%) OF TEN ALGORITHMS ON THE FIRST SYNTHETIC IMAGE WITH DIFFERENT NOISES. THE BEST VALUES ARE HIGHLIGHTED.

Noise	FCM	FCM_S1	FCM_S2	EnFCM	FGFCM	FLICM	NWFCM	KWFLICM	NDFCM	FRFCM
Gaussian 3%	73.70	98.47	98.23	98.86	98.88	99.10	91.91	**99.78**	98.81	**99.78**
Gaussian 5%	67.18	94.53	94.20	97.22	97.18	98.17	89.59	99.52	97.06	**99.64**
Gaussian 10%	59.67	80.53	80.31	88.17	87.46	90.85	89.61	95.45	87.49	**99.04**
Gaussian 15%	56.47	76.39	75.25	80.94	80.46	79.36	**88.35**	85.46	80.60	86.61
Salt & Pepper 10%	94.28	94.85	99.80	95.70	98.65	93.37	99.91	**99.97**	98.60	99.94
Salt & Pepper 20%	83.42	88.31	99.60	86.84	95.27	82.01	99.61	86.88	95.17	**99.86**
Salt & Pepper 30%	77.05	78.42	98.89	83.00	89.29	71.51	98.62	99.31	87.75	**99.78**
Uniform 10%	93.64	97.05	99.85	98.08	98.88	96.53	99.89	**99.96**	98.81	99.93
Uniform 20%	87.14	93.09	99.28	94.82	96.64	90.22	99.42	**99.91**	96.43	99.88
Uniform 30%	80.60	88.30	97.43	90.25	92.58	80.72	97.97	**99.81**	92.19	99.79

TABLE IV
COMPARISON SCORES (S%) OF THE TEN ALGORITHMS ON THE SECOND SYNTHETIC IMAGE WITH DIFFERENT NOISES. THE BEST VALUES ARE HIGHLIGHTED.

Noise	FCM	FCM_S1	FCM_S2	EnFCM	FGFCM	FLICM	NWFCM	KWFLICM	NDFCM	FRFCM
Gaussian 3%	56.69	95.47	95.34	96.64	96.67	97.73	95.31	99.32	96.48	**99.49**
Gaussian 5%	39.57	75.27	75.14	82.89	82.53	88.50	59.97	94.67	82.42	**98.73**
Gaussian 10%	36.61	67.92	68.82	77.04	76.70	82.44	55.63	89.79	76.51	**97.97**
Gaussian 15%	36.31	67.34	68.55	76.98	76.65	81.93	54.81	89.47	76.52	**96.41**
Salt & Pepper 10%	85.65	89.23	99.72	89.78	96.90	84.66	99.77	45.51	96.81	**99.87**
Salt & Pepper 20%	73.56	77.68	99.06	77.55	90.32	69.15	98.92	46.37	89.48	**99.67**
Salt & Pepper 30%	62.33	61.53	96.98	67.86	77.80	53.32	95.36	41.88	76.89	**99.36**
Uniform 10%	86.15	92.79	99.56	95.09	97.12	79.59	99.60	44.67	96.91	**99.84**
Uniform 20%	73.96	84.50	97.93	88.17	91.43	77.99	98.44	52.60	90.85	**99.58**
Uniform 30%	63.25	74.70	93.13	78.68	82.23	63.33	94.81	55.98	81.56	**99.28**

FCM_S1 is incapable of removing Salt & Pepper noise. But FCM_S2 obtains a good segmentation result because median filters employed by FCM_S2 is able to efficiently remove Salt & Pepper noise. NWFCM provides a good segmentation result for images corrupted by Salt & Pepper noise because a weight function incorporating both patch structure information and the local statistics, is introduced in distance measurement between pixels. FLICM and KWFLICM are sensitive to Salt & Pepper noise, which leads to poor results, even KWFLICM obtains a wrong result shown in Fig. 6(j). FGFCM is superior to En-FCM because FGFCM introduces a new factor as a local (both spatial and gray) similarity measure aiming to guarantee both noise-immunity and detail-preservation, and meanwhile remove the empirically-adjusted parameter α for image segmentation. FRFCM has superiorities of both noise-immunity and detail-preservation, and it provides better segmentation results than other algorithms due to the introduction of MR and membership filtering.

From Tables III and IV, we can see that the segmentation accuracy of FRFCM are consistently higher than other algorithms for synthetic images contained different noise. It is obvious that FRFCM is much more robust to different noise than other algorithms. KWFLICM is sensitive to Salt & Pepper and Uniform noise when the noise level is high. FCM_S1 is efficient for images corrupted by Gaussian noise, but FCM_S2 is efficient for images corrupted by Salt & Pepper and Uniform noise. NWFCM is able to provide good segmentation results for image corrupted by Salt & Pepper and Uniform noise, but it is sensitive to Gaussian noise. Both NDFCM and FGFCM are robust to

different noise, and they have close performance according to Tables III and IV.

B. Results on Real Images

Image segmentation plays a key role in medical diagnosis support systems. It is always difficult to segment a medical image because the complexity of medical images such as noise, blur, and intensity nonuniformity. To demonstrate the superiority of the proposed FRFCM, a liver CT image (256×256) including a tumor is considered as a test image in this section. Fig. 7 shows segmentation results of the tumor produced by different algorithms with $c = 5$.

In Fig. 7(a), the tumor is marked by a blue square. Our aim is to segment the tumor from the liver CT image. It is clear that our algorithm shows an excellent performance for the detection of the tumor. Fig. 7 shows that FCM, FCM_S1, FCM_S2, FLICM, NDFCM, and FRFCM are able to segment the tumor accurately shown in Fig. 7(b)–(d), (g), (j), and (k), and EnFCM, FGFCM, NWFCM, and KWFLICM fail to segment the tumor shown in Fig. 7(e), (f), (h), and (i). Compared with the result from FCM, segmentation results from FCM_S1 and FCM_S2 are better, and the segmentation result from FRFCM provides a better visual effect for the tumor. The segmentation result can be used in three-dimensional (3-D) reconstruction of the tumor. And then, by computing the volume of the tumor, a doctor will make a correct diagnosis depending on the variation of the tumor volume.
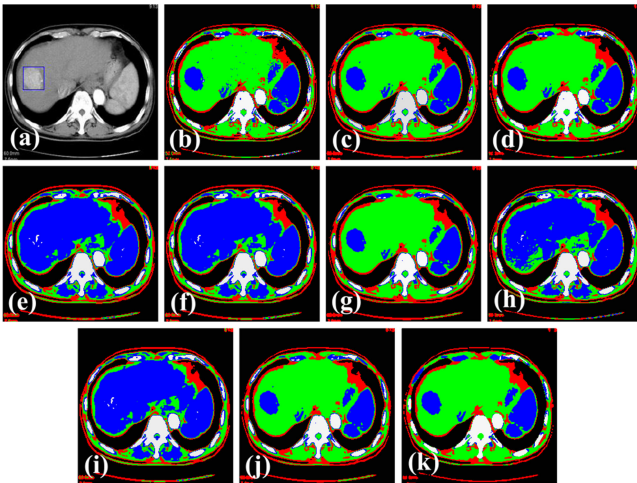
Fig. 7. Comparison of segmentation results on the liver CT image. (a) Original image. (b) FCM result. (c) FCM_S1 result. (d) FCM_S2 result. (e) EnFCM result. (f) FGFCM result. (g) FLICM result. (h) NWFCM result. (i) KWFLICM result. (j) NDFCM result. (k) FRFCM result.

Fig. 8. Comparison of segmentation results on the aurora image. (a) Original image. (b) FCM result. (c) FCM_S1 result. (d) FCM_S2 result. (e) EnFCM result. (f) FGFCM result. (g) FLICM result. (h) NWFCM result. (i) KWFLICM result. (j) NDFCM result. (k) FRFCM result.
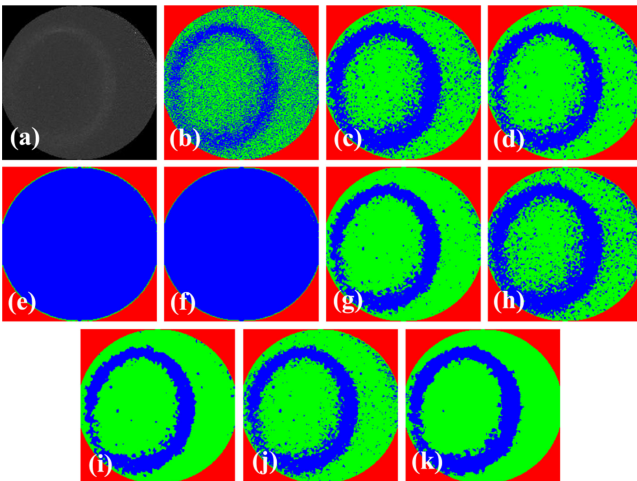
Aurora is formed when solar wind collides with charged particles. It carries important information that reflects the invisible coupling between atmospheric layers. The analysis on aurora images is significant for research on space physics, such as climate changes, global warming, electromagnetic wave interference, etc. [38], [39]. Auroral oval segmentation is a key step in aurora image analysis, and it remains a challenging topic because of random noise, low contrast, and dayglow contamination in Ultraviolet Imager images. To extend the applications of FRFCM in specified image segmentation, an aurora image (228×200) shown in Fig. 8(a) is considered as a tested image. Fig. 8(b)–(k) shows the comparison of segmentation results on auroral oval provided by different algorithms with $c = 3$.

As can be seen from Fig. 8(b) that FCM is sensitive to noise. FCM_S1 and FCM_S2 improve the segmentation result obtained by FCM, but they are unable to segment aurora oval
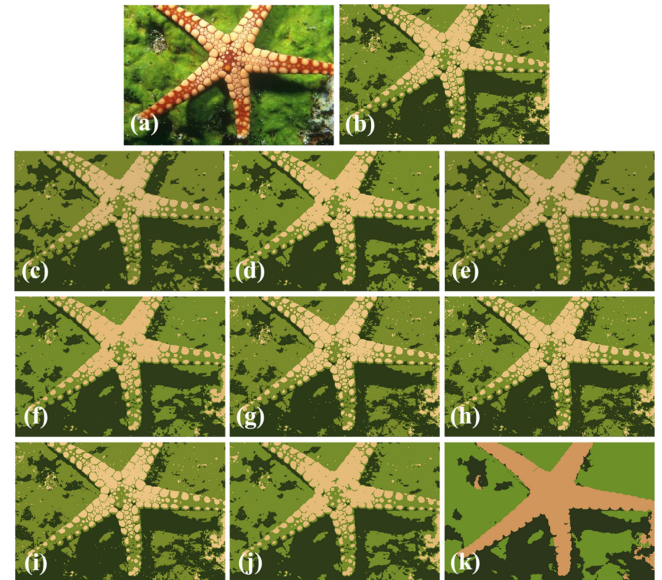

Fig. 9. Comparison of segmentation results on color image "12003" from BSDS500 ($c = 3$). (a) Original image. (b) FCM result. (c) FCM_S1 result. (d) FCM_S2 result. (e) EnFCM result. (f) FGFCM result. (g) FLICM result. (h) NWFCM result. (i) KWFLICM result. (j) NDFCM result. (k) FRFCM result.

efficiently shown in Fig. 8(c) and (d). EnFCM and FGFCM fail to obtain segmentation results of aurora oval shown in Fig. 8(e) and (f). NWFCM and NDFCM are sensitive to noise leading to poor segmentation results shown in Fig. 8(h) and (j). FLICM and KWFLICM provide good segmentation results than other algorithms as shown in Fig. 8(g) and (i). However, they are time-consuming. The proposed FRFCM achieves aurora oval segmentation, shown in Fig. 8(k), with low computation time, and yet the segmentation result is better than other algorithms.

C. Results on Color Images

Most of the improved FCM algorithms are only efficient for gray image segmentation, for it is difficult to obtain local spatial information of color images. However, FCM is able to segment color image with a shorter time, as local spatial information is neglected in FCM. It is easy to extend FCM_S1, FCM_S2, En-FCM, and NDFCM to color image segmentation because image filtering is performed on each channel of color images, respectively. Euclidean distance of pixels (3-D vector) is employed in FLICM, KWFLICM, NWFCM, and FGFCM for color image segmentation, where the local spatial information is computed in each iteration of FLICM and KWFLICM. Thus, FLICM and KWFLICM have a very high computational complexity for color image segmentation. For EnFCM, FGFCM, and FRFCM, the clustering is performed on pixels but not the gray level histogram because it is difficult and complex to obtain the histogram of a color image. In addition, multivariate MR [40] is used in FR-FCM to optimize data distribution, the other steps are similar to gray image segmentation using FRFCM.

In this experiment, the tested images are chosen from the Berkeley Segmentation Dataset (BSDS500) that includes 500 images [41]. The selection of all parameters is the same as
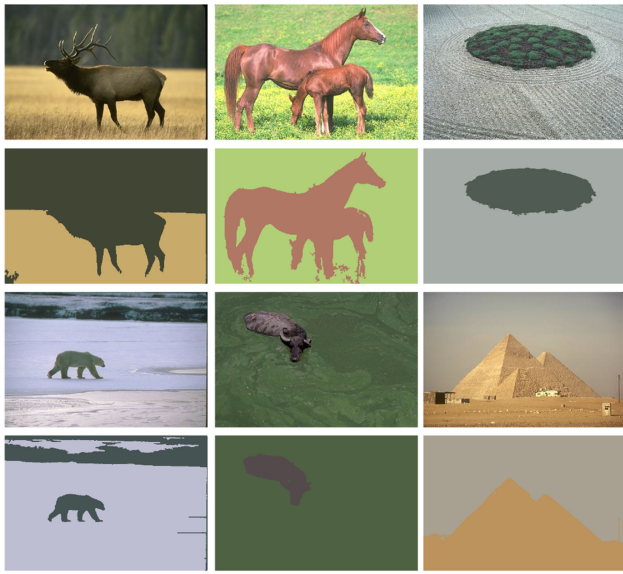
(a)

(b)

Fig. 10. Segmentation results on color images from BSDS500 using FRFCM. (a) c = 2. (b) c = 3.

TABLE V
AVERAGE PERFORMANCE OF TEN ALGORITHMS ON BSDS500 THAT INCLUDES 500 IMAGES (THE BEST VALUES ARE HIGHLIGHTED)

Algorithm	PRI	BDE	CV	VI
FCM	0.72	14.06	0.39	3.15
FCM_S1	0.69	13.45	0.44	2.75
FCM_S2	0.73	13.89	0.40	3.04
EnFCM	0.69	13.47	0.44	2.74
FGFCM	0.73	13.76	0.40	3.06
FLICM	0.72	13.94	0.39	3.11
NWFCM	0.72	13.95	0.39	3.14
KWFLICM	0.72	13.88	0.39	3.10
NDFCM	0.73	13.71	0.40	3.05
FRFCM	**0.76**	**13.03**	**0.46**	**2.59**

TABLE VI
COMPUTATIONAL COMPLEXITY OF TEN ALGORITHMS

Algorithm	Computational complexity
FCM	$O(N \times c \times t)$
FCM_S1	$O(N \times w^2 + N \times c \times t)$
FCM_S2	$O(N \times w^2 + N \times c \times t)$
EnFCM	$O(N \times w^2 + q \times c \times t)$
FGFCM	$O(N \times w^2 + q \times c \times t)$
FLICM	$O(N \times c \times t \times w^2)$
NWFCM	$O(N \times (w+1)^2 + N \times c \times t)$
KWFLICM	$O(N \times (w+1)^2 + N \times c \times t \times w^2)$
NDFCM	$O(N \times w^2 + N \times c \times t)$
FRFCM	$O(N \times w^2 + q \times c \times t)$
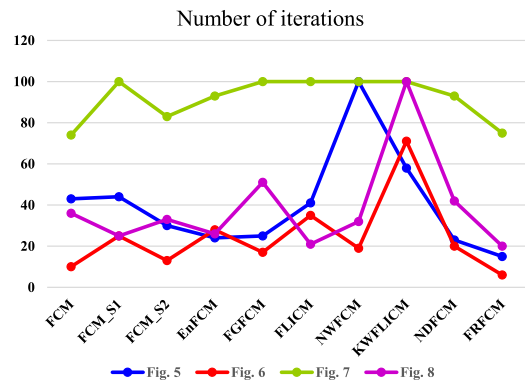
Fig. 11. Comparison of number of iterations of ten algorithms on tested images.

that for gray image segmentation except r in FRFCM ($r = 3$). We conducted experiments and applied these algorithms on BSDS500, and Figs. 9 and 10 show segmentation results. From Fig. 9, we can see that all the algorithms fail to segment the color image except FRFCM. Fig. 9(k) shows that FRFCM obtains excellent segmentation results without changing any parameters. Furthermore, to demonstrate the superiority of FRFCM, we implemented FRFCM on the data set of BSDS500, and some selected segmentation results are shown in Fig. 10. Fig. 10 shows that the segmentation results of different images have accurate contours and we can obtain good object segmentation results

using FRFCM which is simple and significantly fast. It is clear that FRFCM provides excellent segmentation results for color images.

In this paper, four performance measures: probabilistic rand index (PRI) [42], the boundary displacement error (BDE) [43], the covering (CV) [41], and the variation of information (VI) [41] are used to quantitatively evaluate segmentations obtained by different algorithms against the Ground Truth segmentation.

The PRI is a similarity measure that counts the fraction of pairs of pixels whose labels are consistent between the computed segmentation, S', and the corresponding Ground Truth

TABLE VII
COMPARISON OF EXECUTION TIMES (IN SECONDS) OF TEN ALGORITHMS ON TESTED IMAGES. THE BEST VALUES ARE HIGHLIGHTED.

Image	FCM	FCM_S1	FCM_S2	EnFCM	FGFCM	FLICM	NWFCM	KWFLICM	NDFCM	FRFCM
Fig. 5	0.62	0.28	0.23	1.99	12.34	26.04	36.66	50.42	1.85	**0.06**
Fig. 6	0.22	0.28	0.16	0.25	0.27	38.63	13.80	87.49	2.15	**0.03**
Fig. 7	1.66	1.19	1.00	2.25	8.31	110.49	59.06	123.57	3.69	**0.12**
Fig. 8	0.44	0.20	0.21	0.39	5.12	10.07	9.88	54.15	1.48	**0.05**

segmentation, S. PRI can be calculated as follows:

$$\text{PRI}(S, S') = 1 - \left(\sum_i \left(\sum_j p_{ij} \right)^2 - 2 \sum_j \left(\sum_j p_{ij} \right)^2 \right.$$
$$\left. + 2 \sum \sum p_{ij}^2 \right) / N \tag{24}$$

where p_{ij} is the number of pixels in the ith cluster of S and the jth cluster of S', and N is the total number of pixels of the image.

The BDE is an error measure that is used to measure the average displacement error of boundary pixels between two segmentations, and it is defined as

$$\text{BDE}(S, S') = \left(\sum_i^{N_1} d(p_i, S) \right) / N_1 + \left(\sum_i^{N_2} d(p_i, S') / N_2 \right) / 2 \tag{25}$$

where N_1 and N_2 denote the total number of points in the boundary sets S' and S, respectively. d is a distance between a pixel p_i in S' and its closest boundary pixel p in S, and it is defined as follows:

$$d(p_i, S) = \min_{p \in S} \|p_i - p\|. \tag{26}$$

The CV is an overlap measure that can be also used to evaluate the segmentation effect. It is defined as

$$\text{CV}(S \to S') = \left(\sum_{\text{RES}} |R| \cdot \max_{R' \in S'} O(R, R') \right) / N \tag{27}$$

where $O(R, R') = |R \cap R'| / |R \cup R'|$ denotes the overlap between two regions R and R'.

The VI is a similarity measure that is always used to measure the distance between two segmentations in terms of their average conditional entropy given by

$$VI(S, S') = H(S) + H(S') - 2I(S, S') \tag{28}$$

where H and I represent the entropies and mutual information between two segmentations S and S', respectively.

When the final segmentation is close to the Ground Truth segmentation, the PRI and CV is larger while the BDE and VI is smaller. All these algorithms are evaluated on BSDS500, and the average values of PRI, BDE, CV, and VI of segmentation results are given in Table V. c is set from 2 to 6 for each image in BSDS500. We choose a best c corresponding to the highest PRI. The average values of PRI, VI, CV, and BDE obtained by different algorithms are presented in Table V. We can see that our FRFCM clearly outperforms other algorithms on PRI, BDE, CV, and VI values.

From experiments Section IV-A–IV-C, the proposed FR-FCM is able to provide good segmentation results for different typed images. Moreover, it has a better performance than other algorithms.

D. Running Time

Based on the analysis above, the computational complexity of different algorithms are given in Table VI, where N is the number of pixels of an image, c is the number of clustering prototype, t is the iteration number, w is the size of the filtering window, and q is the number of gray levels in the image. Generally, $q \ll N$.

According to Table VI, EnFCM, FGFCM, and FRFCM have low computational complexity due to $q \ll N$ (the gray level of the tested image is $q = 256$, and the number of pixels in the tested image is $N = 256 \times 256$). Moreover, to estimate the practicability of different algorithms, we compared the running time of these algorithms. All experiments are performed on a workstation with an Intel Core (TM) i7-6700, 3.4GHz CPU and 16G memory using MATLAB. Fig. 11 shows number of iterations and Table VII shows execution times (in seconds) of different algorithms on tested images.

From Table VII, it is clear that KWFLICM and FLICM have a very high computational complexity compared to other algorithms. NWFCM is also slow because the computation of neighborhood weights based on patch distance is complex. FCM_S1 and FCM_S2 are fast because mean-filtered images and median-filtered images are computed in advance. EnFCM is fast due to the introduction of gray level and gray level is far less than the number of pixels in an image. FGFCM is not fast because the computation of filtered image is complex. FRFCM only employ MR and membership filtering where MR is performed in advance and median filtering is implemented only once after clustering. Moreover, the idea of histogram is also used in FR-FCM. Therefore, the objective function of FRFCM converges very fast, and FRFCM requires a very small computational time. In addition, we presented the comparison of number of iterations in Fig. 11. We can see that FRFCM requires the least iteration.

In Section IV-C, these algorithms mentioned above are extended to color images, and Figs. 9 and 10 show segmentation results. In contrast with gray image segmentation, they require much time to segment color image due to the increase of dimension of data. Table VIII shows the comparison of computational complexity of different algorithms for Fig. 9.

From Table VIII, we can see that the computational cost of FLICM, KWFLICM, and NWFCM are extremely large for color

TABLE VIII
COMPARISON OF NUMBER OF ITERATIONS AND EXECUTION TIMES (IN SECONDS) OF TEN ALGORITHMS ON COLOR IMAGES (FIG. 9)

	FCM	FCM_S1	FCM_S2	EnFCM	FGFCM	FLICM	NWFCM	KWFLICM	NDFCM	FRFCM
Numbers of iterations	36	100	70	99	46	68	50	76	37	44
Running time	1.52	4.71	3.33	4.466	4.91	366.22	160.78	451.90	12.32	2.73

image segmentation. Although FCM_S1, FCM_S2, EnFCM, FGFCM, NDFCM, and FRFCM have similar computational complexity for color images ($q = N$), FRFCM is significantly faster than these algorithms shown in Table VIII and obtains better segmentation results shown in Figs. 9 and 10.

V. CONCLUSION

In this paper, a significantly fast and robust FRFCM algorithm for image segmentation has been proposed to improve the segmentation quality and reduce the influence of image noise. By introducing MR operation, the local spatial information of images has been utilized to improve segmentation effect. Because MR is able to suppress noise while preserving the contour of objects, a tradeoff has easily been achieved between noise suppression and detail preservation. Moreover, MR is able to provide good reconstructed results for images corrupted by different type of noise. Furthermore, FRFCM employed membership filtering to exploit the local spatial constraint. We demonstrated that membership filtering is able to provide similar results compared with local spatial constraint, but local spatial constraint requires much more time than membership filtering in each iteration. Experimental results show that the proposed FRFCM is able to provide better segmentation results without tuning parameters for different gray or color images.

However, similar to other improved FCM algorithms, the number of clusters is also set experimentally in FRFCM. In the future, we will explore new FCM algorithm that automatically set the number of clusters. In addition, the selection of mask image or marker image is also an open problem; some better results can be obtained by changing mask or marker image.

APPENDIX A

In this appendix, the detailed demonstration that the introduction of local spatial information is similar to membership filter is presented.

Let i denote the sample, k represents the kth cluster, N_i is the neighbor area centered i, c denotes the number of clusters, because $d_{ki} = \|x_i - v_k\|^2$ and $d_{ji} = \|x_i - v_j\|^2$, we can obtain

$$u_{ki} = \frac{\|x_i - v_k\|^{-2/(m-1)}}{\sum_{j=1}^{c} \|x_i - v_j\|^{-2/(m-1)}}$$

$$= \frac{(d_{ki})^{-1/(m-1)}}{\sum_{j=1}^{c} (d_{ji})^{-1/(m-1)}}.$$

If we replace the distance between central pixels and clustering centers with the distance between the neighbors of pixels and clustering centers, then

$$d'_{ki} = \sum_{r \in N_i} w_{kr} d_{kr}$$

$$d'_{ji} = \sum_{r \in N_i} w_{jr} d_{jr}.$$

Therefore, the membership matrix of improved algorithms incorporating neighborhood information (FCM_S, FLICM, KWFLICM) is obtained

$$u'_{ki} = \frac{(d'_{ki})^{-1/(m-1)}}{\sum_{j=1}^{c} (d'_{ji})^{-1/(m-1)}}$$

$$= \frac{\left(\sum_{r \in N_i} w_{kr} d_{kr}\right)^{-1/(m-1)}}{\sum_{j=1}^{c} \left(\sum_{r \in N_i} w_{jr} d_{jr}\right)^{-1/(m-1)}}$$

$$= \frac{(W_{ki} D_{ki})^{-1}}{\sum_{j=1}^{c} (W_{ji} D_{ji})^{-1}}$$

$$= (W_{ki} D_{ki})^{-1} (W'_{ki} D'_{ki})$$

$$= \alpha_1 \frac{D'_{ki}}{D_{ki}}$$

where, $m = 2$, $\alpha_1 = W'_{ki}/W_{ki}$, $W_{ki} D_{ki} = F(\sum_{r \in N_i} w_{kr} d_{kr})$, $W_{ji} D_{ji} = F(\sum_{r \in N_i} w_{jr} d_{jr})$, $W'_{ki} D'_{ki} = F'([\sum_{j=1}^{c} (W_{jr} D_{jr})^{-1}]^{-1})$; $F : (w, d) \to (W, D)$ and $F' : (W, D) \to (W', D')$ are mapping functions.

We consider an idea replacing membership u'_{ki} with its neighborhood membership $u_{kr}, r \in N_i$, i.e.,

$$u''_{ki} = \sum_{r \in N_i} w_{kr} u_{kr}.$$

According to the definition of u_{ki}, we obtain

$$u_{kr} = \frac{(d_{kr})^{-1/(m-1)}}{\sum_{j=1}^{c} (d_{jr})^{-1/(m-1)}}.$$

substituting u_{kr} into u''_{ki}, i.e.,

$$u''_{ki} = \sum_{r \in N_i} w_{kr} \frac{(d_{kr})^{-1/(m-1)}}{\sum_{j=1}^{c} (d_{jr})^{-1/(m-1)}}$$

$$= \sum_{r \in N_i} w_{kr} \frac{(d_{kr})^{-1}}{(D_{kr})^{-1}}$$

$$= w'_{kr} \frac{D'_{kr}}{d'_{kr}}$$

$$= \alpha_2 \frac{D'_{kr}}{D_{kr}}$$

where, $m = 2$, $\alpha_2 = D_{ki} w'_{ki}/d'_{ki}$, $D_{kr} = F_1([\sum_{j=1}^{c}(d_{jr})^{-1}]^{-1})$, $w'_{kr} D'_{ki}/d'_{ki} = F_1'(\sum_{r \in N_i} w_{kr} D_{kr}/d_{kr})$; $F_1 : d \rightarrow D$ and $F_1' : (w, d, D) \rightarrow (w', d'D')$ are mapping functions.

We can see that u''_{ki} and u'_{ki} have the similar form, the only differences between u''_{ki} and u'_{ki} can be found in weighted coefficient, i.e., α_1 and α_2. Therefore, the proposed membership filter is similar to the introduction of local spatial information. ∎

REFERENCES

[1] B. Wang and Z. Tu, "Affinity learning via self-diffusion for image segmentation and clustering," in *Proc. IEEE Conf. Comput. Vis. Pattern Recognit.*, Providence, RI, USA, 2012, pp. 2312–2319.

[2] S. Kim, C. D. Yoo, S. Nowozin, and P. Kohli, "Image segmentation using higher-order correlation clustering," *IEEE Trans. Pattern Anal. Mach. Intell.*, vol. 36, no. 9, pp. 1761–1774, Sep. 2014.

[3] J. Pont-Tuset, P. Arbeláez, J. T. Barron, F. Marques, and J. Malik, "Multiscale combinatorial grouping for image segmentation and object proposal generation," *IEEE Trans. Pattern Anal. Mach. Intell.*, vol. 39, no. 1, pp. 128–140, Jan. 2017.

[4] M. A. Hasnat, O. Alata, and A. Trémeau, "Joint color-spatial-directional clustering and region merging (JCSD-RM) for unsupervised RGB-D image segmentation," *IEEE Trans. Pattern Anal. Mach. Intell.*, vol. 38, no. 11, pp. 2255–2268, Nov. 2016.

[5] C. G. Bampis, P. Maragos, and A. C. Bovik, "Graph-driven diffusion and random walk schemes for image segmentation," *IEEE Trans. Image Process.*, vol. 26, no. 1, pp. 35–50, Jan. 2017.

[6] P. K. Saha, S. Basu, and E. A. Hoffman, "Multiscale Opening of Conjoined Fuzzy Objects: Theory and Applications," *IEEE Trans. Fuzzy Syst.*, vol. 24, no. 5, pp. 1121–1133, Oct. 2016.

[7] F. Masulli and S. Rovetta, "Soft transition from probabilistic to possibilistic fuzzy clustering," *IEEE Trans. Fuzzy Syst.*, vol. 14, no. 4, pp. 516–527, Aug. 2006.

[8] H. Cao, H. W. Deng, and Y. P. Wang, "Segmentation of M-FISH images for improved classification of chromosomes with an adaptive fuzzy c-means clustering algorithm," *IEEE Trans. Fuzzy Syst.*, vol. 20, no. 1, pp. 1–8, Feb. 2012.

[9] A. Javed, Y. C. Kim, M. C. K. Khoo, S. L. D. Ward, and K. S. Nayak, "Dynamic 3-D MR visualization and detection of upper airway obstruction during sleep using region-growing segmentation," *IEEE Trans. Biomed. Eng.*, vol. 63, no. 2, pp. 431–437, Feb. 2016.

[10] V. Grau, A. U. J. Mewes, M. Alcaniz, R. Kikinis, and S. K. Warfield, "Improved watershed transform for medical image segmentation using prior information," *IEEE Trans. Med. Imag.*, vol. 23, no. 4, pp. 447–458, Apr. 2004.

[11] M. Gong, H. Li, X. Zhang, Q. Zhao, and B. Wang, "Nonparametric statistical active contour based on inclusion degree of fuzzy sets," *IEEE Trans. Fuzzy Syst.*, vol. 24, no. 5, pp. 1176–1192, Oct. 2016.

[12] D. Comaniciu and P. Meer, "Mean Shift: A robust approach toward feature space analysis," *IEEE Trans. Pattern Anal. Mach. Intell.*, vol. 24, no. 5, pp. 603–619, May 2002.

[13] D. Mahapatra. "Semi-supervised learning and graph cuts for consensus based medical image segmentation," *Pattern Recognit.*, vol. 63, pp. 700–709, Mar. 2017.

[14] Z. Li and J. Chen, "Superpixel segmentation using linear spectral clustering," in *Proc. IEEE Conf. Comput. Vis. Pattern Recognit.*, Boston, MA, USA, 2015, pp. 1356–1363.

[15] S. P. Chatzis and T. A. Varvarigou, "A fuzzy clustering approach toward hidden markov random field models for enhanced spatially constrained image segmentation," *IEEE Trans. Fuzzy Syst.*, vol. 16, no. 5, pp. 1351–1361, Oct. 2008.

[16] D. Pathak, P. Krähenbühl, and T. Darrell, "Constrained convolutional neural networks for weakly supervised segmentation," in *Proc. IEEE Int. Conf. Comput. Vis.*, Santiago, Chile, 2015, pp. 1796–1804.

[17] J. C. Bezdek, R. Ehrlich, and W. Full, "FCM: The fuzzy c-means clustering algorithm," *Comput. Geosci.*, vol. 10, no. 2-3, pp. 191–203, May 1984.

[18] M. N. Ahmed, S. M. Yamany, N. Mohamed, A. A. Farag, and T. Moriarty, "A modified fuzzy c-means algorithm for bias field estimation and segmentation of MRI data," *IEEE Trans. Med. Imag.*, vol. 21, no. 3, pp. 193–199, Mar. 2002.

[19] S. Chen and D. Zhang, "Robust image segmentation using FCM with spatial constraints based on new kernel-induced distance measure," *IEEE Trans. Syst., Man, Cybern. B, Cybern.*, vol. 34, no. 4, pp. 1907–1916, Aug. 2004.

[20] L. Szilagyi, Z. Benyo, S. M. Szilagyii, and H. S. Adam, "MR brain image segmentation using an enhanced fuzzy c-means algorithm," in *Proc. 25th Annu. Int. Conf. IEEE Eng. Med. Biol. Soc.*, 2003, pp. 17–21.

[21] W. Cai, S. Chen, and D. Zhang, "Fast and robust fuzzy c-means clustering algorithms incorporating local information for image segmentation," *Pattern Recognit.*, vol. 40, no. 3, pp. 825–838, Mar. 2007.

[22] S. Krinidis and V. Chatzis, "A robust fuzzy local information c-means clustering algorithm," *IEEE Trans. Image Process.*, vol. 19, no. 5, pp. 1328–1337, May 2010.

[23] M. Gong, Z. Zhou, and J. Ma, "Change detection in synthetic aperture radar images based on image fusion and fuzzy clustering," *IEEE Trans. Image Process.*, vol. 21, no. 4, pp. 2141–2151, Apr. 2012.

[24] M. Gong, Y. Liang, S. Shi, and J. Ma, "Fuzzy c-means clustering with local information and kernel metric for image segmentation," *IEEE Trans. Image Process.*, vol. 22, no. 2, pp. 573–584, Feb. 2013.

[25] V. May, Y. Keller, N. Sharon, and Y. Shkolnisky, "An algorithm for improving non-local means operators via low-rank approximation," *IEEE Trans. Image Process.*, vol. 25, no. 3, pp. 1340–1353, Mar. 2016.

[26] M. P. Nguyen and S. Y. Chun, "Bounded self-weights estimation method for non-local means image denoising using minimax estimators," *IEEE Trans. Image Process.*, vol. 26, no. 4, pp. 1637–1649, Apr. 2017.

[27] A. M. Saranathan and M. Parente, "Uniformity-based superpixel segmentation of hyperspectral images," *IEEE Geosci. Remote Sens. Lett.*, vol. 54, no. 3, pp. 1419–1430, Mar. 2016.

[28] Z. Zhao, L. Cheng, and G. Cheng, "Neighbourhood weighted fuzzy c-means clustering algorithm for image segmentation," *IET Image Process.*, vol. 8, no. 3, pp. 150–161, Mar. 2014.

[29] F. Guo, X. Wang, and J. Shen, "Adaptive fuzzy c-means algorithm based on local noise detecting for image segmentation," *IET Image Process.*, vol. 10, no. 4, pp. 272–279, Apr. 2016.

[30] L. Vincent, "Morphological grayscale reconstruction in image analysis: Applications and efficient algorithms," *IEEE Trans. Image Process.*, vol. 2, no. 2, pp. 176–201, Apr. 1993.

[31] L. Najman and M. Schmitt, "Geodesic saliency of watershed contours and hierarchical segmentation," *IEEE Trans. Pattern Anal. Mach. Intell.*, vol. 18, no. 12, pp. 1163–1173, Dec. 1996.

[32] M. Gong, L. Su, M. Jia, and W. Chen, "Fuzzy clustering with a modified MRF energy function for change detection in synthetic aperture radar images," *IEEE Trans. Fuzzy Syst.*, vol. 22, no. 1, pp. 98–109, Feb. 2014.

[33] G. Teodoro, T. Pan, T. M. Kurc, L. Cooper, J. Kong, and J. H. Saltz, "A fast parallel implementation of queue-based morphological reconstruction using GPUs," Center Comprehensive Informat., Emory Univ., Atlanta, GA, USA, Tech. Rep. CCI-TR-2012-2, 2012.

[34] A. K. Nandi, A. J. Basel, and F. Rui, *Integrative Cluster Analysis in Bioinformatics*. Hoboken, NJ, USA: Wiley, 2015.

[35] A. M. Mendonca and A. Campilho, "Segmentation of retinal blood vessels by combining the detection of centerlines and morphological reconstruction," *IEEE Trans. Med. Imag.*, vol. 25, no. 9, pp. 1200–1213, Sep. 2006.

[36] J. J. Chen, C. R. Su, W. E. L. Grimson, J. L. Liu, and D. H. Shiue, "Object segmentation of database images by dual multiscale morphological reconstructions and retrieval applications," *IEEE Trans. Image Process.*, vol. 21, no. 2, pp. 828–843, Feb. 2012.

[37] P. Soille, *Morphological Image Analysis: Principles and Applications*. New York, NY, USA: Springer-Verlag, 2013.

[38] X. Yang, X. Gao, D. Tao, and X. Li, "Improving level set method for fast auroral oval segmentation," *IEEE Trans. Image Process.*, vol. 23, no. 7, pp. 2854–2865, Jul. 2014.

[39] X. Yang, X. Gao, D. Tao, X. Li, B. Han, and J. Li, "Shape-constrained sparse and low-rank decomposition for auroral substorm detection," *IEEE Trans. Neural Netw. Learn. Syst.*, vol. 27, no. 1, pp. 32–46, Jan. 2016.

[40] T. Lei, Y. Zhang, Y. Wang, S. Liu, and Z. Guo, "A conditionally invariant mathematical morphological framework for color images," *Inf. Sci.*, vol. 387, pp. 34–52, May 2017.

[41] P. Arbelaez, M. Maire, C. Fowlkes, and J. Malik, "Contour detection and hierarchical image segmentation," *IEEE Trans. Pattern Anal. Mach. Intell.*, vol. 33, no. 5, pp. 898–916, May 2011.

[42] R. Unnikrishnan, C. Pantofaru, and M. Hebert, "Toward objective evaluation of image segmentation algorithms," *IEEE Trans. Pattern Anal. Mach. Intell.*, vol. 29, no. 6, pp. 929–944, Jun. 2007.

[43] X. Wang, Y. Tang, S. Masnou, and L. Chen, "A global/local affinity graph for image segmentation," *IEEE Trans. Image Process.*, vol. 24, no. 4, pp. 1399–1411, Apr. 2015.

Tao Lei received the Ph.D. degree in information and communication engineering from Northwestern Polytechnical University, Xi'an, China, in 2011.

From 2012 to 2014, he was a Postdoctoral Research Fellow with the School of Electronics and Information, Northwestern Polytechnical University. From 2015 to 2016, he was a Visiting Scholar with the Quantum Computation and Intelligent Systems group at University of Technology Sydney, Sydney, Australia. From July to October in 2017, he was a Visiting Scholar with the Department of Electronic and Computer Engineering, Brunel University London, London, U.K. He is currently a Professor with the College of Electrical and Information Engineering, Shaanxi University of Science and Technology, Xi'an, China. His current research interests include image processing, pattern recognition, and machine learning.

Xiaohong Jia received the M.S. degree in signal and information processing from Lanzhou Jiaotong University, Lanzhou, China, in 2017. He is currently working toward the Ph.D. degree at the College of Electronical and Information Engineering, Shaanxi University of Science and Technology, Xi'an, China.

His current research interests include image processing and pattern recognition.

Yanning Zhang (M'08–SM'12) received the B.S. degree in electronic and engineering from Dalian University of Technology, Dalian, China, in 1988, and the Ph.D. degree in signal and information processing from Northwestern Polytechnical University, Xi'an, China, in 1996.

She is currently a Professor with the School of Computer Science, Northwestern Polytechnical University. Her current research interests include computer vision and pattern recognition, image and video processing, and intelligent information processing.

Prof. Zhang was the Organization Chair of the Asian Conference on Computer Vision 2009. She served as the Program Committee Chair of several international conferences.

Lifeng He (SM'12) received the B.E. degree from the Northwest Institute of Light Industry, Shaanxi, China, in 1982, a second B.E. degree from Xi'an Jiaotong University, Xi'an, China, in 1986, the M.S. and Ph.D. degrees in AI and computer science from Nagoya Institute of Technology, Nagoya, Japan, in 1994 and 1997, respectively.

He is a Guest Professor with the Shaanxi University of Science and Technology, Xi'an, China, and a Professor with the Aichi Prefectural University, Nagakute, Japan. From September 2006 to May 2007, he worked with the University of Chicago, Chicago, IL, USA, as a Research Associate. His research interests include image processing, computer vision, automated reasoning, pattern recognition, information retrieval, and artificial intelligence.

Hongying Meng (M'10–SM'17) received the Ph.D. degree in communication and electronic systems from Xi'an Jiaotong University, Xi'an China, in 1998.

He is currently a Senior Lecturer with the Department of Electronic and Computer Engineering, Brunel University London, London, U.K. He is also a Member of Institute of Environment, Health and Societies, Human Centred Design Institute, and Wireless Networks and Communications Research Center, Brunel University London. He is a Fellow of The Higher Education Academy and a Member of Engineering Professors Council in U.K. His research interests include digital signal processing, affective computing, machine learning, human computer interaction, computer vision, and embedded systems with over 90 publications in these areas.

Dr. Meng was the recipient of the International Audio/Visual Emotion Challenges AVEC2011 and AVEC2013 prizes, respectively, for his audio-based and video-based emotion recognition systems.

Asoke K. Nandi (F'11) received the Ph.D. degree in physics from the University of Cambridge (Trinity College), Cambridge, U.K.

He held academic positions in several universities, including Oxford (U.K.), Imperial College London (U.K.), Strathclyde (U.K.), and Liverpool (U.K.) as well as Finland Distinguished Professorship in Jyvaskyla (Finland). In 2013, he moved to Brunel University London, London, U.K., to become the Chair and Head of Electronic and Computer Engineering. He is a Distinguished Visiting Professor with Tongji University, Shanghai, China, and an Adjunct Professor with the University of Calgary, Calgary, AB, Canada. In 1983, he codiscovered the three fundamental particles known as W^+, W^-, and Z^0 (by the UA1 team at CERN), providing the evidence for the unification of the electromagnetic and weak forces, for which the Nobel Committee for Physics in 1984 awarded the prize to two of his team leaders for their decisive contributions. He has made many fundamental theoretical and algorithmic contributions to many aspects of signal processing and machine learning. He has much expertise in "Big Data," dealing with heterogeneous data, and extracting information from multiple datasets obtained in different laboratories and different times. He has authored more than 550 technical publications, including 220 journal papers as well as four books, entitled *Automatic Modulation Classification: Principles, Algorithms and Applications* (Wiley, 2015), *Integrative Cluster Analysis in Bioinformatics* (Wiley, 2015), *Blind Estimation Using Higher-Order Statistics* (Springer, 1999), and *Automatic Modulation Recognition of Communications Signals* (Springer, 1996). Recently, he has authored or coauthored *Blood*, *International Journal of Neural Systems, BMC Bioinformatics*, IEEE TRANSACTIONS ON WIRELESS COMMUNICATIONS, *NeuroImage, PLoS One, Royal Society Interface, Mechanical systems and Signal Processing*, and *Molecular Cancer*. The h-index of his publications is 67 (Google Scholar) and ERDOS number is 2. His current research interests include signal processing and machine learning, with applications to communications, gene expression data, functional magnetic resonance data, and biomedical data.

Prof. Nandi is a Fellow of the Royal Academy of Engineering, London, U.K. and also a Fellow of seven other institutions including the IEEE and the IET. He was the recipient of the Institute of Electrical and Electronics Engineers (USA) Heinrich Hertz Award in 2012, the Glory of Bengal Award for his outstanding achievements in scientific research in 2010, the Water Arbitration Prize of the Institution of Mechanical Engineers (UK) in 1999, and the Mountbatten Premium, Division Award of the Electronics and Communications Division, of the Institution of Electrical Engineers (UK) in 1998. He is an IEEE EMBS Distinguished Lecturer (2018–2019).